Electron-Transfer Processes of Cytochrome *c* at Interfaces. New Insights by Surface-Enhanced Resonance Raman Spectroscopy

DANIEL H. MURGIDA* AND
PETER HILDEBRANDT

Technische Universität Berlin, Institut für Chemie, Max Volmer Laboratorium für Biophysikalische Chemie, Sekr. PC 14, Strasse des 17. Juni 135, D-10623 Berlin, Germany

FIGURE 1. Schematic representation of the potential distribution across a lipid bilayer.

ABSTRACT

The heme protein cytochrome *c* acts as an electron carrier at the mitochondrial-membrane interface and thus exerts its function under the influence of strong electric fields. To assess possible consequences of electric fields on the redox processes of cytochrome *c*, the protein can be immobilized to self-assembled monolayers on electrodes and studied by surface-enhanced resonance Raman spectroscopy. Such model systems may mimic some essential features of biological interfaces including local electric field strengths. It is shown that physiologically relevant electric field strengths can effectively modulate the electron-transfer dynamics and induce conformational transitions.

Introduction

Most of the natural reactions of redox proteins occur at or in membranes under conditions that are distinctly different from those in solution. First, mobilities of the proteins are strongly restricted either for integral proteins because of embedment into the lipid bilayer or, for soluble ones, because of binding to the membrane surface or to the solvent-exposed part of the membrane-bound reaction partners. Second, dielectric constants along the electron transfer (ET) pathway may vary substantially. Third, different ion concentrations on both sides of the membrane generate a potential drop across the membrane, which as well as the inhomogeneous charge distribution within the lipid bilayer and the integral proteins, can lead to very high electric field strengths at the binding domains

Daniel H. Murgida obtained his Ph.D. in chemistry in 1997 from the Universidad de Buenos Aires under the supervision of Prof. Rosa Erra-Balsells. In 1999, he joined the group of Prof. Peter Hildebrandt at the Max Planck Institute für Strahlenchemie as an Alexander von Humboldt fellow, and in 2001, he moved to the Instituto de Tecnologia Química e Biológica (Universidade Nova de Lisboa) (ITQB) as an Auxiliary Researcher. Since 2003, he is the Staff Scientist at the Technische Universität Berlin and Visiting Professor at ITQB.

Peter Hildebrandt received his Ph.D. in chemistry from the Universität Göttingen in 1985. After a post-doc stay in Princeton, he worked at the Max Planck Institutes in Göttingen and in Mülheim a.d.R., where he became a Staff Scientist. In 2001, he was appointed as Investigador Coordenador at the Instituto de Tecnologia Química e Biológica (Universidade Nova de Lisboa). Since 2003, he is a Full Professor for Physical Chemistry and Biophysical Chemistry at the Technische Universität Berlin and Visiting Professor at ITQB.
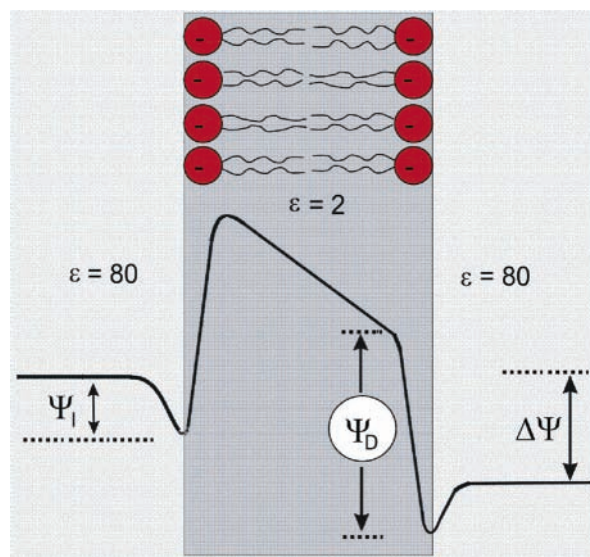
of the reacting proteins (Figure 1).[1] Such field strengths that can reach values up to 10^9 V/m may have a pronounced effect on the dynamics of charge-transfer processes and the structures of the proteins, which can result in reaction mechanisms that differ from those in solution.

To address these questions, new approaches are required that are capable of probing reactions and structural properties of proteins at interfaces. In this respect, electrochemical interfaces represent convenient model systems because they can mimic the charge distribution of the membrane/solution interface specifically upon appropriate coating of the electrodes. Processes of proteins immobilized on coated electrodes can be studied by electrochemical techniques whose performance has been substantially improved such that it is possible to analyze thermodynamics and dynamics of the redox reactions of protein monolayers.[2,3] However, electrochemical methods do not provide structural information about the species involved and thus allow only indirect conclusions about the possible coupling of Faradaic and non-Faradaic processes. As a powerful alternative, surface-enhanced resonance Raman (SERR) spectroscopy can be employed. This technique takes advantage of the molecular resonance Raman (RR) and the surface-enhanced Raman (SER) effects such that, upon appropriate choice of the excitation line, it is possible to probe selectively the vibrational spectra of the prosthetic group solely of the immobilized protein, and thus, it affords detailed information on the redox site structure.[4] SERR spectroscopy can be performed in the stationary[5] and, by combination with the potential-jump technique, in the time-resolved (TR) mode[6,7] such that equilibria and kinetics of potential-dependent interfacial processes can be monitored based on the characteristic vibrational signatures of the species involved.

* To whom correspondence should be addressed. Phone: +49-30-31426500. E-mail: dh.murgida@tu-berlin.de.
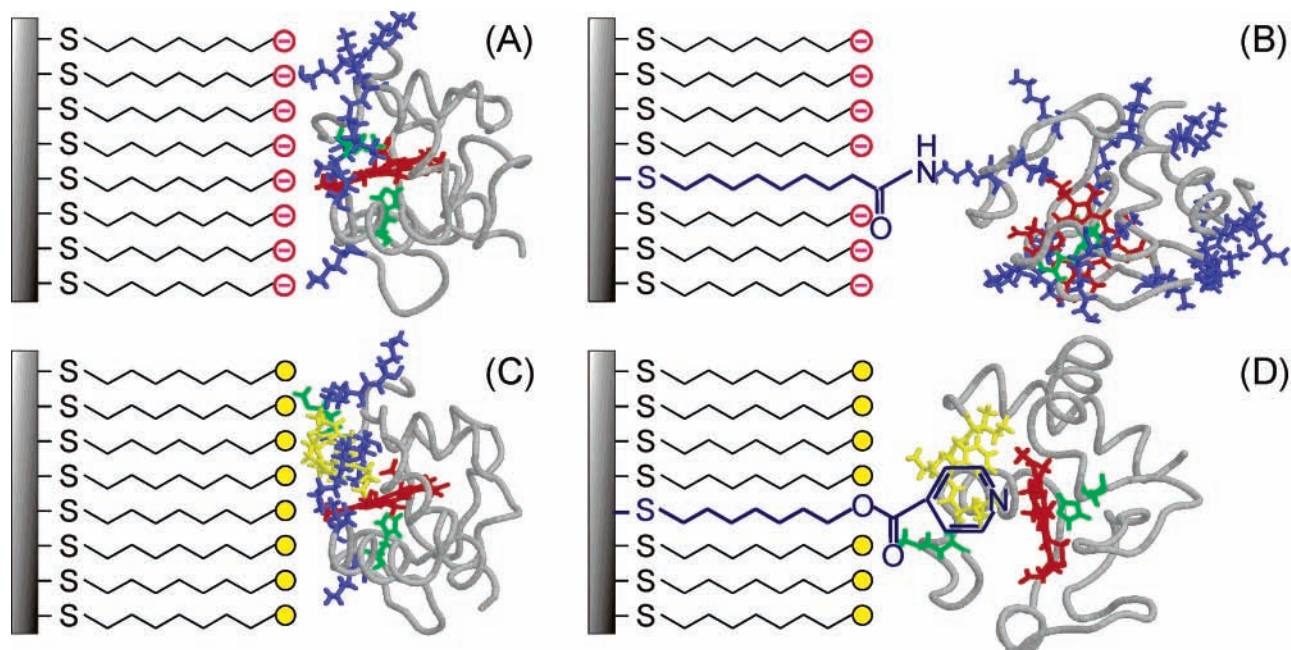
FIGURE 2. Different modes of Cyt *c* immobilization using SAMs of bifunctional alkanethiols with (A) anionic phosphonate (PO_3–SAM) or carboxylate headgroups (CO_2–SAM) for electrostatic binding via surface lysines (blue), (B) carboxylate headgroups to be cross-linked to amino groups of the lysine residues for covalent binding, (C) methyl headgroups (CH_3–SAM) for hydrophobic binding via the peptide segment 81–85 (yellow), and (D) pyridinyl headgroups (Py–SAM) for coordinative binding to the heme (red).

Most of the SERR spectroscopic work has been carried out with cytochrome *c* (Cyt *c*), because structural and dynamic properties of this water-soluble heme protein are known in great detail.[8] Cyt *c* is an electron carrier in aerobic respiration transferring electrons from cytochrome *c* reductase to cytochrome *c* oxidase (CcO), where the electrons are utilized to reduce oxygen to water. The reaction partners of Cyt *c* are membrane-bound enzyme complexes integrated in the mitochondrial membrane in close vicinity to each other, such that Cyt *c* most likely migrates between both reaction sites via lateral diffusion along the membrane surface. Thus, it lives and works in the membrane/solution interface. Consequently, a detailed investigation of the ET of Cyt *c* at model interfaces may contribute to a better understanding of the natural redox process of this protein in particular and, possibly, to identify the parameters governing interfacial charge-transfer processes in general.

Immobilization Strategies

The exposed heme edge of Cyt *c* is enclosed by a ring-shaped arrangement of seven lysine residues that are positively charged at pH 7.[9] Because of the asymmetric distribution of basic and acid residues, the protein exhibits a large dipole moment with its positive end pointing through the center of the ring of lysines.[10] This part of the protein surface constitutes the binding domain for interacting with the (anionic) docking sites of natural partner proteins as well as with negatively charged surfaces in general.[9,11,12] Hence, immobilization of Cyt *c* can preferentially be achieved via electrostatic forces if the electrode surface is negatively charged.

At potentials above the potential of zero charge (E_{pzc}; ca. −0.9 V versus Ag/AgCl), the Ag electrode carries a positive charge, which however, is generally overcompensated by specifically adsorbed anions (e.g., sulfate), forming a negatively charged layer to which Cyt *c* is adsorbed.[5,6,13,14] Alternatively, the metal surface can be coated by self-assembled monolayers (SAM) of ω-functionalized alkanethiols carrying charged headgroups such as carboxylate (CO_2–SAM)[15–20] or phosphonate groups (PO_3–SAM) (Figure 2).[21] This approach is particularly interesting because it allows varying the charge density of the monolayer surface and the separation of the bound protein from the electrode. Furthermore, SAMs provide biocompatible surfaces because they avoid irreversible structural changes of the immobilized protein (denaturation), which slowly but inevitably occur upon direct adsorption to the bare (anion-coated) Ag electrode.[14] In this sense, SAM-coated electrodes can also be considered as simple models for biomembranes because they mimic important features of lipid layers such as the hydrophobic core and the charged headgroups.

The positively charged lysines around the heme edge ensure that Cyt *c* binds to anionic SAMs via the front surface of the protein. Because not all of these lysine residues can simultaneously interact with anionic headgroups, various slightly different orientations of the immobilized protein are possible. However, analysis of the ET kinetics by TR SERR spectroscopy[15], as well as the ideal Nernstian behavior[16], indicates that at potentials > ca. −0.05 V Cyt *c* adopts a largely uniform orientation that is favorable for a rapid ET. Evidently, this preferential configuration is established because of the orientation of the large molecule dipole moment in the interfacial
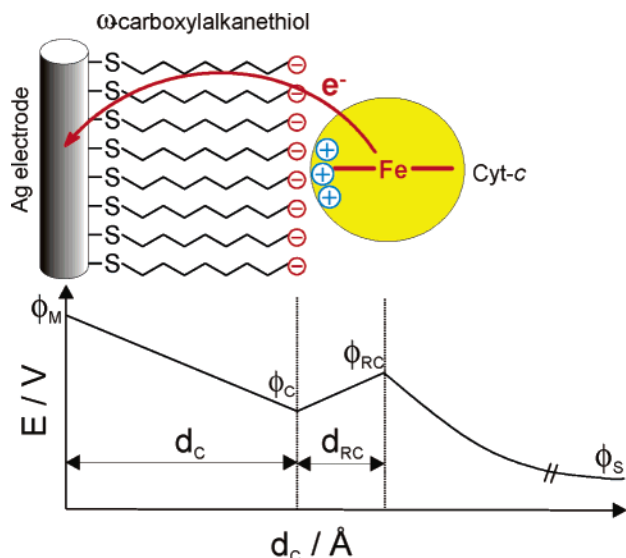
FIGURE 3. Schematic representation of the potential distribution at the Ag/SAM/Cyt *c*/solution interfaces.

electric field. As the field strength decreases upon approaching E_{pzc}, the orientational distribution of the immobilized protein becomes heterogeneous at potentials < -0.05 V.[15,21]

The ring-shape arrangement of the lysines in the binding domain encloses a hydrophobic patch involving the peptide segment 81−85 that is located above the heme plane, i.e., on the side of axial Met-80 ligand. Evidence has been provided that hydrophobic interactions in the electrostatically stabilized complex of Cyt *c* with CcO are essential for the natural redox process.[22] To explore the role of hydrophobic interactions, SAMs of methyl-terminated alkanethiols (CH$_3$−SAM) can be formed to which Cyt *c* is immobilized via the peptide segment 81−85 that may partially penetrate into the hydrophobic monolayer.[23] Alternative approaches to immobilize Cyt *c* are based on the formation of covalent or coordinative bonds. Covalent attachment is achieved by cross-linking reagents that afford the formation of amide bonds between the amino side functions of the lysines on the protein surface and the carboxyl headgroups of CO$_2$−SAMs.[17] A coordinative bond to the heme iron is formed when Cyt *c* interacts with SAMs carrying N ligands as headgroups, like pyridinyl-terminated alkanethiols (Py−SAM).[24,25] These residues can effectively replace the natural Met-80 ligand and thus constitute a direct molecular wire from the redox center to the metal electrode.

Interfacial Electric Fields

A simple electrostatic model (Figure 3) has been developed for estimating the potential drops across the electrode/SAM/protein interfaces and thus the electric field strength experienced by the immobilized Cyt *c*.[16,26,27] Despite the underlying approximation involved, the model provides a consistent description of experimentally accessible parameters such as the charge densities on the SAM surface (σ_c) and at the redox site (σ_{RC}), as well as the potential drop at the redox site $|E_{RC}|$, which increases with

SAM thickness d_c.[16] The electric field strength E_F at the protein-binding site depends on these parameters according to

$$E_F(d_c) = \frac{\epsilon_0 \epsilon_s \kappa E_{RC} - \sigma_c - \sigma_{RC}}{\epsilon_0 \epsilon_c} \quad (1)$$

where κ is the inverse Debye length and ϵ_s and ϵ_c denote the dielectric constants of the solution and the SAM, respectively. For CO$_2$−SAMs, the electric field strength at the Cyt *c*-binding site is in the order of 10^9 V m^{-1},[16] which is comparable to that estimated for biological membranes in the vicinity of charged lipid headgroups.[1] Higher field strengths are predicted for PO$_3$−SAM and sulfate monolayers for which $|\sigma_c|$ is distinctly larger, whereas the field strength is strongly reduced in the case of hydrophobic headgroups ($\sigma_c = 0$ C/m^2).

Structural Changes of the Immobilized Protein

Immobilization of Cyt *c* on coated Ag electrodes may lead to reversible structural changes that include the heme coordination pattern. Specifically, the Met-80 ligand is removed from the sixth coordination site, which remains either vacant (five-coordinated high spin, 5cHS) or is occupied by a His (six-coordinated low spin, 6cLS) or, particularly, at pH < 7, by a water molecule.[13,14,16] Changes of spin and coordination configuration as well as the oxidation state give rise to frequency shifts and intensity variations in the SERR spectra specifically in the marker band region, thereby constituting characteristic fingerprints for each species (Figure 4).[28]

The species that lack the Met-80 ligand are denoted as the B2 state, in distinction to the B1 state in which the native structure of Cyt *c* is fully preserved. The reaction scheme for the conformational transitions between B1 and B2, as well as between the B2 substates (Figure 5), holds for electrostatic and hydrophobic binding to electrodes and, moreover, to model systems in solution such as phospholipid vesicles or micelles. However, conformational equilibria and evidently the mechanisms of the conformational changes are different for electrostatic and hydrophobic binding. Upon electrostatic binding, salt bridges between lysine residues in the binding domain and the anionic groups on the coated electrode, together with the interfacial electric field, cause a destabilization of the heme crevice, which eventually leads to the dissociation of the Met-80 bond from the heme iron. On the other hand, hydrophobic interactions between methyl headgroups of the SAM and the hydrophobic patch close to the exposed heme edge may induce a displacement of the peptide segment 81−85 away from the heme such that it partially penetrates into the monolayer.[23] Such a displacement would immediately affect the coordinative bond of Met-80 that is directly linked to this segment. After the dissociation of the Fe-Met bond, a His residue can bind to the heme, specifically in the oxidized form.

On the basis of a thorough comparative analysis using a variety of spectroscopic techniques, it was concluded that this His is the same His (His-33 or His-26) that
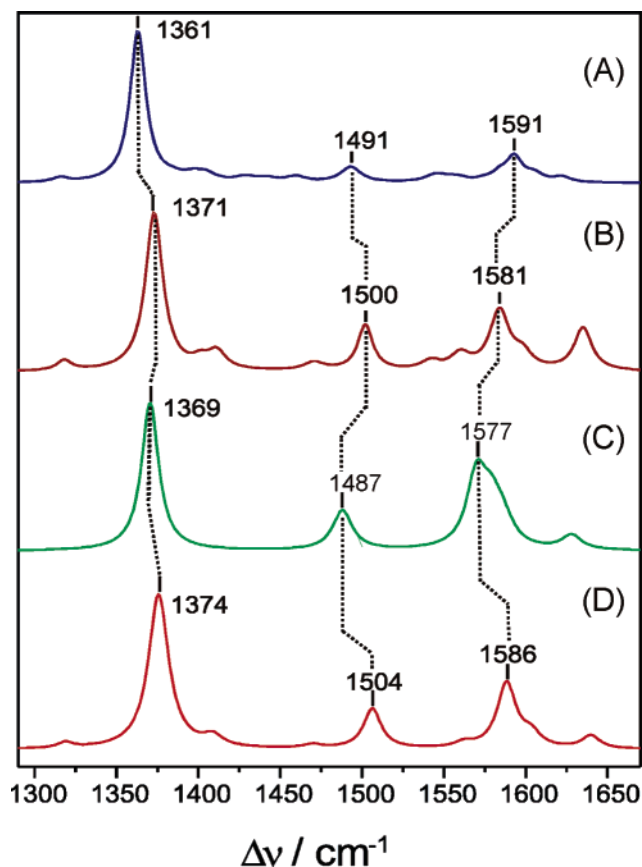
FIGURE 4. SERR spectra of different oxidation, spin, and coordination states of Cyt *c* immobilized on a CO_2—SAM measured with 413-nm excitation. (A) B1[6cLS]^{red}, (B) B1[6cLS]^{ox}, (C) B2[5cHS]^{ox}, and (D) B2[6cLS]^{ox}.
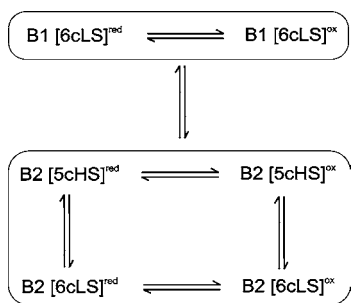

FIGURE 5. Reaction scheme of Cyt *c* bound to charged or hydrophobic surfaces.

coordinates to the heme iron during unfolding and folding processes of Cyt *c*, where the bisHis-coordinated (ferric) complex forms a kinetic trap.[28,29] Furthermore, it was found that the formation of B2 does not involve notable changes in the secondary structure but is associated with alterations of tertiary structure, which involve the movement of the peptide segment 30(20) − 49 to bring His-33 (His-26) in proximity to the heme.[28]

In contrast to the reversible B1 → B2 transition, specific immobilization conditions may lead to slow and irreversible structural changes of ferric Cyt *c* presumably associated with the replacement of the His-18 ligand of the heme. This denaturation process may interfere with the B2/B1 equilibrium when Cyt *c* is immobilized on CH_3—SAMs[23] or on sulfate monolayers at potentials > 0.15 V.[14]

Conformational and Redox Equilibria

When Cyt *c* is adsorbed on a bare (sulfate-coated) Ag electrode, all B1 and B2 species are populated to such an extent that allows for the determination of the redox potentials for all three redox couples.[14] The Nernstian plots derived from the analyses of the potential-dependent SERR spectra reveal a nearly ideal behavior with redox potentials of 0.064, −0.38, and −0.34 V for the B1, B2-[6cLS], and B2[5cHS] couples, respectively. The redox potential of B1 is very similar to the value in solution (0.06 V),[8] which is in line with the structural identity of B1 and the protein in solution. The same redox potential was found for B1 on CO_2—SAMs taking into account the d_c-dependent interfacial potential drop.[16] The negative shifts in the redox potentials of the B2 species can be rationalized in terms of the change of the ligation pattern and the heme-pocket structure.[5,14]

In contrast to electrostatic adsorption, covalently attached Cyt *c* (B1) displays a nonideal electrochemical behavior.[17] Most likely, the cross-linking reactions involve various lysine residues leading to a distribution of orientations that may also include electrochemically less active or inactive species.

For Cyt *c* immobilized on Py—SAM electrodes, the SERR spectroscopic analysis indicates that the immobilized protein forms a potential-dependent coordination equilibrium, which is dominated by the Py-coordinated 6cLS configuration in the oxidized form and a 5cHS species in the reduced form.[24] SERR spectra and the redox potential of the 6cLS couple (−0.24 V) are similar to the corresponding data for Py—Cyt *c* complexes in solution. The potential dependence of the coordination equilibrium is consistent with the higher affinity of pyridine for the ferric protein. Formation of the immobilized Py—Cyt *c* complex, however, is only efficient when the pyridinyl-terminated thiols are diluted in methyl-terminated thiols, implying that additional hydrophobic interactions with the peptide segment 81−85 are essential for stabilizing the complex.[24]

The reaction scheme in Figure 5 implies potential-dependent conformational equilibria. On sulfate monolayers and PO_3—SAM, B1[6cLS]^{red} is the predominant form at negative potentials, while at potentials above 0.05 V oxidized B2 species prevail.[14] When the fact that $|\sigma_c|$ and thus the electric field strength increase with increasing potential is taken into account, one can rationalize the potential dependence of the B2/B1 equilibrium as well as the fact that high potentials (>0.15 V) on sulfate-coated Ag eventually lead to irreversible structural changes for a small fraction of the adsorbed molecules.[14]

Using CO_2—SAMs of different chain lengths as expressed by the number of carbon atoms *n*, the electric field dependence of the B2/B1 equilibrium can be analyzed quantitatively. For relatively long chain lengths (*n* ≥ 11), the adsorbed protein exists in the B1 state, independent of the redox state and the applied potential.[16] For *n* < 11 and electrode potentials of ca. 0.0 V, the contribution of the B2 species steadily increases upon decreasing *n* and thus with increasing electric field
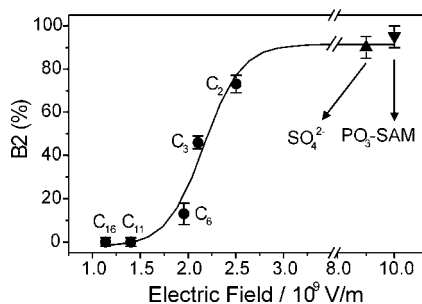
FIGURE 6. Relative concentrations of B2^{ox} of Cyt *c* on various anionic surfaces as determined by SERR spectroscopy. C$_n$ refers to CO$_2$–SAMs of *n* total carbon atoms.

strength (eq 1).[16] Even larger portions of B2^{ox} are found on sulfate monolayers and PO$_3$–SAM (Figure 6).[21]

According to eq 1, a decrease of the protein-surface coverage lowers σ_{RC} and causes a concomitant increase of σ_c. Because both quantities have opposite signs, an increase of the electric field strength and thus an increase of the B2^{ox}/B1^{ox} ratio is in fact observed at CO$_2$–SAM (*n* = 3) upon lowering the concentration of Cyt *c*.

When the experiments are carried out at potentials distinctly lower than the redox potential of B1, the only species that can be detected is the reduced form of B1 and no contributions of the reduced B2 are observed. This finding can be rationalized based on the relative stabilities of the coordinative bonds, which are higher for the Fe–Met and Fe–His bonds in the ferrous and ferric forms, respectively, and the decrease in electric field strength with decreasing potential.[15]

Upon immobilization of Cyt *c* to hydrophobic CH$_3$–SAM,[23] the B2/B1 equilibria do not depend on the chain length of the alkanethiols for *n* > 2 because electric field strengths are very small (σ_c = 0) and a different mechanism is operative for the formation of the B2 state. Only on short coatings (*n* = 2), a larger portion of the native B1 state is found at potentials around ca. 0.0 V compared to monolayers with longer chains, where B2^{ox} prevails. Evidently, a minimum chain length is required to accommodate the hydrophobic peptide segment 81–85 in the monolayer as an essential step for the B2 formation and possibly also for a largely uniform orientation. For longer chain lengths, B2^{ox} and B1^{red} are the prevailing forms at potentials above and below −0.2 V, respectively, whereas B2^{red} and B1^{ox} cannot be detected at any potential. Thus, for these systems, only the coupled redox /conformational equilibria can be probed rather than pure redox processes.[23]

Dynamics of the Interfacial Electron-Transfer Reactions.

On CO$_2$–SAMs and at high protein coverage, Cyt *c* exists largely in the native B1 state and the contribution of the conformational B2 state is negligibly small even at short chain lengths and positive potentials.[16,21] Under these conditions, potential jumps induce only the ET reaction between the adsorbed B1 and the electrode such that TR SERR spectra probe a one-step relaxation process. The
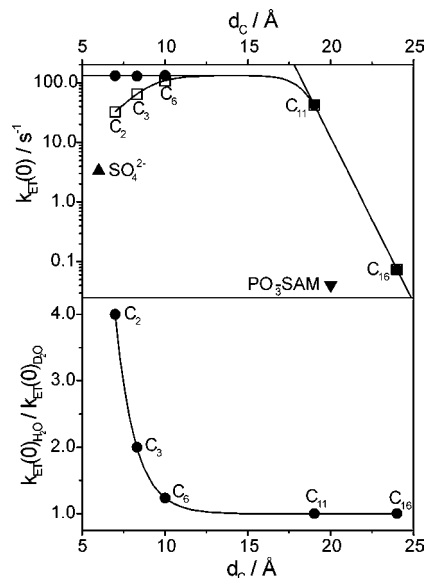
FIGURE 7. Distance dependence of $k_{ET}(0)$ (top) and the KIE (bottom) for Cyt *c* (B1) electrostatically adsorbed on various SAM- and sulfate-coated Ag electrodes. C$_n$ refers to CO$_2$–SAMs of *n* total carbon atoms.

quantitative analysis of the TR spectra that were measured as a function of the delay time δ with respect to the potential jump affords the ET rate constants. For potential jumps to the redox potential corresponding to a driving force of 0 electronvolt (eV), one obtains the formal heterogeneous ET rate constant k_{ET}.

For B1 on CO$_2$–SAMs, k_{ET} was determined as a function of the chain length (Figure 7).[18] For long-range ET in the nonadiabatic regime, one expects an exponential increase of k_{ET} with decreasing d_c (or *n*) according to

$$k_{ET} = A \exp(-d_c\beta) \qquad (2)$$

where β is the tunneling parameter.[30] The increase of k_{ET} by a factor of ca. 600 from *n* = 16 to 11 corresponds to A = 1.45 × 10^{12} s^{-1} and β = 1.28 Å^{-1} (eq 2).[18] Both values are in line with previous results for long-range ET of different redox proteins in solution.[31] This agreement, albeit based on only two data points, indicates that at long distances, corresponding to low electric field strengths, the rate constants refer to an electron tunneling process. However, at shorter distances, k_{ET} only slightly increases to 134 s^{-1} at *n* = 6 and remains essentially unchanged at *n* = 3 and 2.[18] This deviation from the "normal" exponential distance dependence indicates that at high electric fields the rate-limiting step is no longer electron tunneling but must be due to a different process.

ET at Low Electric Fields. The reorganization energy λ of the ET reaction can be determined in the electron-tunneling regime, i.e., at long SAM lengths. In one approach, the driving force, corresponding to the overpotential $\eta = E_f − E°$, is systematically varied and the rate constants $k_{ET}(\eta)$ determined from the TR SERR experiments are analyzed according to the semiclassical Marcus theory[32]

$$k_{ET}(\eta) = k_{ET}(0) \, \frac{1 - erf \dfrac{F(\eta + \lambda)}{2\sqrt{F\lambda RT}}}{1 - erf \dfrac{F\lambda}{2\sqrt{F\lambda RT}}} \qquad (3)$$

where $k_{ET}(0)$ refers to the rate constant at a driving force of 0 eV (Figure 8). Equation 3 provides an excellent fit to the experimental data with $\lambda = 0.22$ eV.[20] This value is in good agreement with the results obtained from temperature-dependent time-resolved and stationary SERR spectroscopic measurements.[19]

The reorganization energy of the electrostatically immobilized Cyt *c* is distinctly lower than the value determined for the protein in solution (ca. 0.6 eV).[33] This decrease is primarily ascribed to the solvent reorganization energy, which is lowered because of the (partial) exclusion of water molecules from the binding domain. Furthermore, for the remaining solvent molecules in the electrical double layer of the SAM/solvent interface that contribute to the hydration shell of the immobilized protein, the static dielectric constant is substantially smaller compared to the bulk solution.[19]

ET at High Electric Fields. The nonexponential distance dependence of k_{ET} of Cyt *c* immobilized on short CO_2−SAMs (Figure 7) has also been observed in electrochemical experiments and debated controversially.[18,19,25,34] In contrast to long chain lengths, the ET rate of Cyt *c* at short CO_2−SAM is independent of the overpotential (Figure 8).[19,21] Thus, the largely constant value for k_{ET} determined for $n \leq 6$ [18] cannot be taken as an indication for a change from nonadiabatic to adiabatic regime as it was suggested for Cyt *c* directly wired to the electrode via Py−SAMs.[25] Instead, for CO_2−SAM with $n \leq 6$ or high electric fields, a different process that is not ET becomes rate-limiting.

In view of the viscosity dependence of k_{ET} in the nonexponential regime ($n < 11$), this limiting step was attributed to a reorientation of the immobilized protein.[34] However, this explanation cannot account for the H/D kinetic isotope effect (KIE) observed in TR SERR experiments.[18] It was found that the onset of the nonexponential distance dependence is accompanied by a steadily increasing KIE from 1.2 ($n = 6$) to 4.0 ($n = 2$), whereas in the electron-tunneling regime ($n \geq 11$) $k_{ET}(0)$ is the same in H_2O and D_2O (Figure 7).[18] Thus, the KIE on the measured ET rate implies that the interfacial process involves the transfer of proton(s), which becomes rate-limiting at short distances.

On the other hand, an increase of the viscosity affects the ET rate at values that are much larger than that of D_2O (1.2 cP), and a decrease of the ET rate by a factor of 4, corresponding to the KIE on CO_2−SAM with $n = 2$, requires a viscosity as high as 1.7 cP.[21] Thus, the results indicate that the interfacial ET includes protein motion *and* a proton transfer (PT) process. This PT may be associated with redox-linked alterations of the hydrogen-bonded interactions in the protein and in the protein/SAM interface. In fact, the hydrogen-bond network in the interior of Cyt *c* differs in the ferric and the ferrous form[35]
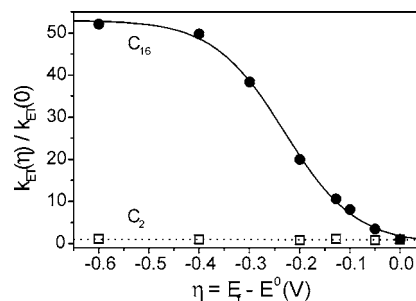

FIGURE 8. Overpotential dependence of k_{ET} for Cyt *c* (B1) bound to CO_2−SAM with $n = 16$ (●) and $n = 2$ (□). The solid line represents a fit of eq 3 to the experimental data that were obtained from TR SERR experiments.

such that a rearrangement of the hydrogen bonds is an essential part of the structural reorganization that is a prerequisite for electron tunneling.

This PT becomes rate-limiting only under the specific reaction conditions for Cyt *c* adsorbed at the electrode interface, i.e., under the influence of strong electric fields, because in solution, no KIE has been observed. A possible explanation is that the activation energy for the PT steps increases with the electric field strength, i.e., with a decreasing thickness of the SAM. In fact, temperature-dependent TR SERR measurements yield substantially higher activation enthalpies for the redox process of Cyt *c* at $n = 3$ (24.2 and 34.3 kJ mol^{-1} in H_2O and in D_2O, respectively) than at $n = 16$ (13 kJ mol^{-1} in both solvents).[19] The ratio of the preexponential factors at $n = 3$ is $A(D_2O)/A(H_2O) = 0.82$, whereas $\Delta H°$ and $\Delta S°$ of the *entire* redox process are largely independent of the electric field and the solvent.[19] The large difference in the activation enthalpies of 10.1 kJ/mol for $n = 3$ cannot be understood within the framework of semiclassical over-the-barrier H/D transfer.[18,19] Therefore, a quantum-mechanical-tunneling contribution for the PT process[36] has to be considered for the interfacial redox process of Cyt *c*.

In D_2O, the distance-dependence of k_{ET} at CO_2−SAM displays a maximum at $n = 6$ in contrast to the rate constant in H_2O that remains largely unchanged for $n \leq 6$ (Figure 7).[18] Evidently, the electric field strength at CO2−SAMs that can be obtained even for $n = 2$ is not sufficiently strong to raise the energy barrier for the PT step such that the k_{ET} decreases again. This decrease, however, is observed for PO_3−SAM (0.045 s^{-1}),[21] for which the ET rate constant was found to be ca. 1000 times smaller than the one for a carboxyl-terminated SAM of similar length. Conversely, this low value as well as the one for the sulfate-coated electrode (3.3 s^{-1})[14] can be understood based on an electric-field-dependent activation barrier for rate-limiting PT steps (Figure 9).

Hydrophobic SAM coatings represent the other extreme case, i.e., very low electric fields. Although in such systems, ET reactions are strongly coupled with conformational transitions, it is at least possible to estimate the order of magnitude of the ET rate constant that indicates a normal exponential distance dependence at least down to $n = 5$.[23]
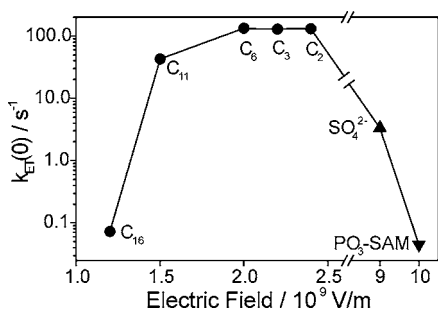
FIGURE 9. Electric field dependence of $k_{ET}(0)$ for Cyt *c* (B1) electrostatically adsorbed on various SAM- and sulfate-coated Ag electrodes. C_n refers to CO_2—SAMs of *n* total carbon atoms.

Conformational Dynamics

Also the conformational dynamics are controlled by the electric field. Whereas on hydrophobic coatings specific conformational transitions, i.e., the formation of the B1^{red} or B2^{ox}, occur within less than 1 ms;[23] substantially slower rates are observed at high electric fields at least for the transition to the ferric B2 state.[14,21] For Cyt *c* immobilized on CO_2—SAM with $n = 2$ at low protein coverage, a detailed analysis for the transition from B1^{red} to B2^{ox} reveals that the initial fast ET to B1^{ox} ($k_{ET} = 130$ s^{-1}) is followed by the dissociation of the Met-80 ligand from the heme with a rate constant of ca. 25 s^{-1} up to a relative contribution that corresponds to a change of the concentration of B2^{ox}5cHS of ca. 5%.[21] On the time scale of seconds, the remaining B1^{ox} decays to the 5cHS and 6cLS configurations of B2^{ox} that coexist in a rapid equilibrium. Thus, the main part of the conformational transition occurs at a rate that is ca. 6000 times slower than the redox reaction, indicating that the electric field, local electrostatic interactions, or both effects impose substantial constraints on the dynamics of the peptide segments that are involved. The slow conformational transitions are affected by the viscosity in the solution but do not exhibit an H/D KIE.[21]

Electric-Field-Dependent Modulation of Biological Redox Processes

Although the complexity of the supramolecular structure and self-organization of amphiphiles is much lower in the coatings of electrodes than in biological membranes, local electric field strengths experienced by peripherally bound or integral proteins may be comparable in both cases (Figure 1).[1,16] In addition, some characteristic features of the interfacial processes of Cyt *c* on electrodes have already been identified for this protein interacting with its natural reaction partner CcO. First, the B2 state has been detected in the fully oxidized complex with CcO even in the absence of external electric fields, and the portion of B2 correlates with the enzymatic activity of CcO toward Cyt *c*.[11] Second, the enzymatic reaction can be drastically slowed for CcO reconstituted in phospholipid vesicles when the transmembrane potential and thus the electric field strength are increased.[37] Thus, it may well be that similar to coated electrodes the electric field represents a

crucial determinant for the redox process of Cyt *c* also under physiological conditions.

A possible mechanism that has been proposed previously suggests that the alterations of the transmembrane potential brought about by ion gradients may modulate the local electrostatic interactions of Cyt *c* in the complex with CcO.[19] At low potentials, corresponding to weak electric fields, ET and conformational transitions are sufficiently fast to form B2^{ox} within the lifetime of the Cyt *c*/CcO complex, after interprotein ET. Thus, unproductive rereduction of the Cyt *c* is avoided. When the transmembrane potential during the enzymatic turnover is increased, the increasing electric field may eventually block ET and conformational transitions such that the enzymatic activity is strongly reduced. Thus, this effect may constitute the basis for a regulatory mechanism.

The SERR spectroscopic studies described in this Account may not only contribute to the elucidation of the natural redox process of Cyt *c* because the dramatic electric field effects on the structure as well as on the reaction mechanism and dynamics are not a unique property of this specific protein. Electric field modulation has also been observed for other redox and nonredox proteins as discussed previously.[38] Therefore, the electric field must be considered as an essential parameter for controlling interfacial processes in electrochemistry and biology in general.

References

(1) Clarke, R. J. The Dipole Potential of Phospholipid Membranes and Methods for its Detection. *Adv. Colloid Interface Sci.* **2001**, *89*, 263–281.
(2) Armstrong, F. A.; Wilson, G. S. Recent Developments in Faradaic Bioelectrochemistry. *Electrochim. Acta* **2000**, *45*, 2623–2645.
(3) *Electroanalytical Methods for Biological Material*; Brajter-Toth, A., Chambers, J. Q., Eds.; Marcel Dekker: New York, 2002.
(4) Cotton, T. M.; Kim, J. H.; Holt, R. E. Surface-Enhanced Resonance Raman Scattering (SERRS) Spectroscopy: A Probe of Biomolecular Structure and Bonding at Surfaces. In *Advances in Biophysical Chemistry*; Bush, C. A., Ed.; JAI Press Inc.: London, U.K., 1992; Vol. II, pp 115–147.
(5) Hildebrandt, P.; Stockburger, M. Cytochrome *c* at Charged Interfaces. 1. Conformational and Redox Equilibria at Electrode/Electrolyte Interface Probed by Surface-Enhanced Resonance Raman Spectroscopy. *Biochemistry* **1989**, *28*, 6710–6721.
(6) Wackerbarth, H.; Klar, U.; Günther, W.; Hildebrandt, P. Novel Time-Resolved Surface-Enhanced (Resonance) Raman Spectroscopic Technique for Studying the Dynamics of Interfacial Processes: Application to the Electron-Transfer Reaction of Cytochrome *c* at a Silver Electrode. *Appl. Spectrosc.* **1999**, *53*, 283–291.
(7) Lecomte, S.; Wackerbarth, H.; Soulimane, T.; Buse, G.; Hildebrandt, P. Time-Resolved Surface-Enhanced Resonance Raman Spectroscopy for Studying Electron-Transfer Dynamics of Heme Proteins. *J. Am. Chem. Soc.* **1998**, *120*, 7381–7382.
(8) *Cytochrome c—A Multidisciplinary Approach*; Scott, R. A.; Mauk, A. G., Eds.; University Science Books: Sausalito, CA, 1995.
(9) Banci, L.; Bertini, I.; Rosato, A.; Varani, G. Mitochondrial Cytochromes *c*: A Comparative Analysis. *J. Biol. Inorg. Chem.* **1999**, *4*, 824–837.
(10) Koppenol, W. H.; Margoliash, E. The Asymmetric Distribution of Charges on the Surface of Horse Cytochrome *c*. *J. Biol. Chem.* **1982**, *257*, 4426–4437.
(11) Döpner, S.; Hildebrandt, P.; Rosell, F. I.; Mauk, A. G.; von Walter, M.; Buse, G.; Soulimane, T. The Structural and Functional Role of Lysine Residues in the Binding Domain of Cytochrome *c* in the Electron Transfer to Cytochrome *c* Oxidase. *Eur. J. Biochem.* **1999**, *261*, 379–391.

(12) Roberts, V. A.; Pique, M. E. Definition of the Interaction Domain for Cytochrome *c* on Cytochrome *c* Oxidase—III. Prediction of the Docked Complex by a Complete, Systematic Search. *J. Biol. Chem.* **1999**, *274*, 38051—38060.

(13) Wackerbarth, H.; Murgida, D. H.; Oellerich, S.; Döpner, S.; Rivas, L.; Hildebrandt, P. Dynamics and Mechanism of the Electron-Transfer Process of Cytochrome *c* Probed by Resonance Raman and Surface Enhanced Resonance Raman Spectroscopy. *J. Mol. Struct.* **2001**, *563*, 51—59.

(14) Wackerbarth, H.; Hildebrandt, P. Redox and Conformational Equilibria and Dynamics of Cytochrome *c* at High Electric Fields. *Chem. Phys. Chem.* **2003**, *4*, 714—724.

(15) Murgida, D. H.; Hildebrandt, P. Active-Site Structure and Dynamics of Cytochrome *c* Immobilized on Self-Assembled Monolayers— A Time-Resolved Surface Enhanced Resonance Raman Spectroscopic Study. *Angew. Chem., Int. Ed.* **2001**, *40*, 728—731.

(16) Murgida, D. H.; Hildebrandt, P. Heterogeneous Electron Transfer of Cytochrome *c* on Coated Silver Electrodes. Electric Field Effects on Structure and Redox Potential. *J. Phys. Chem. B* **2001**, *105*, 1578—1586.

(17) Murgida, D. H.; Hildebrandt, P. The Heterogeneous Electron Transfer of Cytochrome *c* Adsorbed on Ag Electrodes Coated with Omega-Carboxyl Alkanethiols. A Surface Enhanced Resonance Raman Spectroscopic Study. *J. Mol. Struct.* **2001**, *565*, 97—100.

(18) Murgida, D. H.; Hildebrandt, P. Proton-Coupled Electron Transfer of Cytochrome *c. J. Am. Chem. Soc.* **2001**, *123*, 4062—4068.

(19) Murgida, D. H.; Hildebrandt, P. Electrostatic-Field Dependent Activation Energies Modulate Electron Transfer of Cytochrome *c. J. Phys. Chem. B* **2002**, *106*, 12814—12819.

(20) Hildebrandt, P.; Murgida, D. H. Electron-Transfer Dynamics of Cytochrome *c* Bound to Self-Assembled Monolayers on Silver Electrodes. *Bioelectrochem. Bioenerg.* **2002**, *55*, 139—143.

(21) Rivas, L.; Marti, M.; Smith, A.; Murgida, D. H.; Hildebrandt, P. Unpublished data.

(22) Witt, H.; Malatesta, F.; Nicoletti, F.; Brunori, M.; Ludwig, B. Tryptophan 121 of Subunit II Is the Electron Entry Site to Cytochrome-*c* Oxidase in Paracoccus Denitrificans—Involvement of a Hydrophobic Patch in the Docking Reaction. *J. Biol. Chem.* **1998**, *273*, 5132—5136.

(23) Rivas, L.; Murgida, D. H.; Hildebrandt, P. Conformational and Redox Equilibria and Dynamics of Cytochrome *c* Immobilized on Electrodes Via Hydrophobic Interactions. *J. Phys. Chem. B* **2002**, *106*, 4823—4830.

(24) Murgida, D. H.; Hildebrandt, P.; Wei, J.; He, Y. F.; Haiying Liu; Waldeck, D. H. Surface-Enhanced Resonance Raman Spectroscopic and Electrochemical Study of Cytochrome *c* Bound on Electrodes through Coordination with Pyridinyl-Terminated Self-Assembled Monolayers. *J. Phys. Chem. B* **2004**, *108*, 2261—2269.

(25) Wei, J. J.; Liu, H. Y.; Khoshtariya, D. E.; Yamamoto, H.; Dick, A.; Waldeck, D. H. Electron-Transfer Dynamics of Cytochrome *c*: A Change in the Reaction Mechanism with Distance. *Angew. Chem., Int. Ed.* **2002**, *41*, 4700—4703.

(26) Smith, C. P.; White, H. S. Theory of the Interfacial Potential Distribution and Reversible Voltametric Response of Electrodes Coated with Electroactive Molecular Films. *Anal. Chem.* **1992**, *64*, 2398—2405.

(27) Lecomte, S.; Hildebrandt, P.; Soulimane, T. Dynamics of the Heterogeneous Electron-Transfer Reaction of Cytochrome c_{552} from Thermus Thermophilus. A Time-Resolved Surface-Enhanced Resonance Raman Spectroscopic Study. *J. Phys. Chem. B* **1999**, *103*, 10053—10064.

(28) Oellerich, S.; Wackerbarth, H.; Hildebrandt, P. Spectroscopic Characterization of Nonnative Conformational States of Cytochrome *c. J. Phys. Chem. B* **2002**, *106*, 6566—6580.

(29) Yeh, S. R.; Han, S. W.; Rousseau, D. L. Cytochrome *c* Folding and Unfolding: A Biphasic Mechanism. *Acc. Chem. Res.* **1998**, *31*, 727—736.

(30) Marcus, R. A.; Sutin, N. Electron Transfer in Chemistry and Biology. *Biochim. Biophys. Acta* **1985**, *811*, 265—322.

(31) Gray, H. B.; Winkler, J. R. Electron Transfer in Proteins. *Annu. Rev. Biochem.* **1996**, *256*, 537—561.

(32) Nahir, T. M.; Clark, R. A.; Bowden, E. F. Linear-Sweep Voltammetry of Irreversible Electron-Transfer in Surface-Confined Species Using the Marcus Theory. *Anal. Chem.* **1994**, *66*, 2595—2598.

(33) Cheng, J.; Terrettaz, S.; Blankman, J. I.; Muller, C. J.; Dangi, B.; Guiles, R. D. Electrochemical Comparison of Heme Proteins by Insulated Electrode Voltammetry. *Isr. J. Chem.* **1997**, *37*, 259—266.

(34) Avila, A.; Gregory, B. W.; Niki, K.; Cotton, T. M. An Electrochemical Approach to Investigate Gated Electron-Transfer Using a Physiological Model System: Cytochrome *c* Immobilized on Carboxylic Acid-Terminated Alkanethiol Self-Assembled Monolayers on Gold Electrodes. *J. Phys. Chem. B* **2000**, *104*, 2759—2766.

(35) Gao, Y.; McLendon, G.; Pielak, G. J.; Williams, R. J. P. Electron Proton Coupling in Cytochrome-*c* Studied Using Protein Variants. *Eur. J. Biochem.* **1992**, *204*, 337—352.

(36) Krishtalik, L. I. The Mechanism of the Proton Transfer: An Outline. *Biochim. Biophys. Acta* **2000**, *1458*, 6—27.

(37) Moroney, P. M.; Scholes, T. A.; Hinkle, P. C. Effect of Membrane-Potential and pH Gradient on Electron Transfer in Cytochrome-Oxidase. *Biochemistry* **1984**, *23*, 4991—4997.

(38) Rivas, L.; Hippler-Mreyen, S.; Engelhard, M.; Hildebrandt, P. Electric-Field-Dependent Decays of Two Spectroscopically Different M-States of Photosensory Rhodopsin II From *Natronobacterium pharaonis. Biophys. J.* **2003**, *84*, 3864—3873.